JCTC Journal of Chemical Theory and Computation

Article

pubs.acs.org/JCTC

Opsin Effect on the Electronic Structure of the Retinylidene Chromophore in Rhodopsin

Eduardo M. Sproviero*

Department of Chemistry & Biochemistry, University of the Sciences in Philadelphia, 600 South 43rd Street, Philadelphia, Pennsylvania 19104-4495, United States

ABSTRACT: Direct examination of experimental NMR parameters combined with electronic structure analysis was used to provide a first-principle interpretation of NMR experiments and give a precise evaluation of how the electronic perturbation of the protein environment affects the electronic properties of the retinylidene chromophere in rhodopsin. To this end, we pursued a theoretical analysis using a combination of tools including quantum mechanics/molecular mechanics (QM/MM) at the Density Functional Theory (DFT) level, in conjunction with gauge independent atomic orbital (GIAO) calculations of ^{13}C NMR chemical shieldings and $^{1}J_{CC}$ spin−spin coupling constants obtained with the Coupled Perturbed DFT (CPDFT) method. The opsin effect on the retinylidene chromophere is interpreted as an inductive effect of Glu-113 which readjusts the weighting factors of resonance substructures of the conjugated chain of the chromophere. These changes give a rationalization to the alternating effect of the ^{13}C chemical shifts magnitudes when comparing the retinylidene chromophere in the presence and absence of the protein environment. Conversely, perturbation of π orbitals has little to no effect over ^{1}J $^{13}C-^{13}C$ spin−spin coupling constants, as they are mainly dominated by the Fermi contact term, and hence the counteraion effect is restricted to the vicinity of the perturbation. Thus, the apparent contradiction between experimental findings based on chemical shifts (deep penetration) and one-bond *J*-couplings (localized effects of the protonated Schiff base at the chain terminus) is in fact a consequence of different properties responding differently to the same external perturbation.

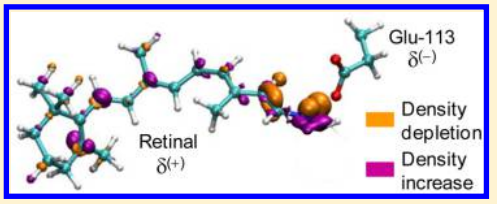

1. INTRODUCTION

Understanding the structure−function relationship of G-protein-coupled receptors (GPCRs) at the detailed molecular level is a subject of great interest, since GPCRs are the essential components of a variety of biological signal transmission pathways.[1] The membrane glycoprotein rhodopsin is a prototypical GPCR present in the rod cells of the retina, responsible for turning on the signaling transmission cascade in the vertebrate vision process. Rhodopsin consists of two building blocks, an opsin protein called scotopsin and a covalently bound cofactor, retinal (retinaldehyde). The structure of rhodopsin consists of seven transmembrane protein helices bound by a protonated Schiff-base (PSB) linkage through Lys-296 to the 11-Z-retinylidene chromophore. The Schiff-based linkage between Lys-296 and the chromophore bears a net positive charge NH^{+}, compensated by the Glu-113 counteranion, forming a salt bridge.[2] Isomerization of 11-*cis*-retinal into an all-*E*-retinylidene configuration by light induces a conformational change in the opsin that activates the associated G protein and triggers a second messenger cascade.[3]

Since its inception, the relation between Nuclear Magnetic Resonance (NMR) parameters with molecular structure has been an essential part of modern chemistry. The availability of suitable computational and experimental methods to obtain both magnetic shieldings and coupling constants allows a better understanding of the correlation between NMR parameters and molecular or electronic structure. The magnetic shielding, which defines the experimentally measured chemical shift δ, is a local phenomenon that reflects the surroundings of the nucleus under study. It has been used to study conformations in solution or in the crystalline state, to study dynamic effects,[4] and to explore nuclear electronic environments.[5] The components of the magnetic shielding tensor of a given nucleus can differ by several hundreds of parts per million within the same compound, particularly when π systems are present. Over the past decade, NMR shielding tensors have been calculated routinely for a vast range of systems.[6] On the other side, the main components of the tensor can be found experimentally from NMR measurements in solid state, liquid crystals, or other spectroscopic techniques.[7]

The other common NMR parameter, the indirect nuclear spin−spin coupling constant, is extremely sensitive to the local molecular geometry and has been used for a long time for structural assignments. In contrast to NMR shieldings, *ab initio* calculations of spin−spin coupling constants are computationally expensive, requiring roughly twice as much as a frequency job,[8] and have been carried out only lately in systems containing a few tens of heavy atoms.[6a,9] Progress in NMR experimental techniques, and in particular the use of high magnetic fields, has made possible the accurate measurement of coupling constants in a variety of molecular environments, including systems of substantial size, such as proteins, nucleic acids, and their complexes.[10]

Received: July 14, 2014
Published: February 4, 2015

DOI: 10.1021/ct500612n
J. Chem. Theory Comput. 2015, 11, 1206−1219

In rhodopsin, NMR estimations of $^{13}C-^{13}C$ distances, dipole−dipole couplings, and ^{13}C chemical shifts within the retinylidene chain suggest that the PSB positive charge is partially delocalized and stabilized near the isomerization site by polar protein side chains and an associated water molecule[11] or penetrates deeper into the conjugated chain.[12] However, ^{1}J $^{13}C-^{13}C$ spin−spin coupling constants,[13] X-ray diffraction,[14] and density functional calculations[14] provide no indication that the protein environment significantly perturbs the electronic structure of the conjugated system, apart from the localized effects of the PSB at the imine terminus, making the bond alternation in the retinylidene chromophore insensitive to the protein environment. The aim of this work is to show that in both cases the main influence of the protein comes from the PSB counterion. However, the counterion affects the magnitude of certain properties only in the vicinity of the imine terminus, while other properties manifest the counterion influence deeper into the retinal chain, up to the ionone ring.

NMR parameters and electronic structure descriptors were used to analyze how they depend on each other. Then those parameters were evaluated in the retinilydene chromophore of rhodopsin with and without the protein environment, using the Quantum Mechanics/Molecular Mechanics (QM/MM) hybrid method, based on the successful application of this approach to study spectroscopy and mechanisms of various rhodopsins.[15] To understand which particular molecular property of the environment affects the retinal, electrostatic and electron delocalization[16] effects were selectively isolated from the protein surroundings and the response of the NMR parameters determined. The use of this strategy allows identification of how the protein environment affects various NMR parameters. It will be shown that the apparent contradiction in determining the degree of delocalization of the effect of the protein environment into the chromophore chain is mainly due to a different response of the chemical shifts and coupling constants to the same electronic redistribution of the polyene chain.

This paper is organized as follows. Section 2 describes the methodology, including a description of the Quantum Mechanics/Molecular Mechanics (QM/MM) approach, and the calculation of chemical shifts, nuclear spin−spin coupling constants, and electronic structure parameters. In section 3, how these parameters are affected by electronegative substituents within the chain terminus, the PSB counteranion, and the protein environment is discussed. In section 4, how the molecular properties interrelate with NMR parameters is described. Section 5 summarizes and concludes.

2. METHODS

2.1. Protein and Small Molecule Models. A description of the optimized QM/MM model and method used to study the retinylidene chromophore in rhodopsin (model **1**) can be found elsewhere.[12b,17] Here, a brief summary of the underlying methodology is included as follows. The QM/MM model investigated in this article is based on the refinement of the crystal structure of bovine rhodopsin (Protein Data Bank, i.e., PDB, accession code 1F88, monomer A), solved at 2.8 Å resolution.[18] To this model, two additional water molecules were added, in accord with the 2.6 Å resolution 1L9H PDB crystal structure (monomer A) of Okada et al.[19]

The rhodopsin cavity is set neutral, consistent with experiments.[20] The optimized model of rhodopsin was prepared considering standard protonation of all titratable groups, which means that residues relevant to this work, Ser186 and Cys187, are neutral. Amino acid residues Glu-122 and Asp-83, all within the protein core, are assumed to be neutral, as indicated by FTIR experiments[20] and UV−vis spectroscopic measurements of site-directed mutants.[21] The protonation state of Glu-181 is still controversial because Fourier transform infrared spectroscopy measurements, ^{13}C NMR, and some theoretical analysis indicated this residue to be charged (unprotonated),[22] while preresonance Raman and UV−vis spectra, as well as some theoretical analysis, were in favor of the uncharged state.[23] Glu-181 was set as protonated in the simulations, consistently with our previous calculations,[12b,17] and in line with recent studies, which state that the protonation state of Glu-181 affects neither significantly ^{1}H and ^{13}C NMR chemical shifts[24] nor the relative stabilities of the S_1 and S_2 single excited states and the photoisomerization path of the retinal chromophore.[15e]

The Schiff-based linkage between Lys-296 and the chromophore bears a net positive charge NH^{+}, compensated by the Glu-113 counterion. The regular ends of the protein and the artificial ends due to the missing or incomplete amino acids from the X-ray structures in the third cytoplasmic loop (236−239) and in the C-terminal tail (328−348) are capped with NH^{+3} and CO^{-2}.

QM/MM hybrid calculations were carried out at the ONIOM Electronic-Embedding[25] (B3LYP/6-31G*:Amber) level of theory using Gaussian 03.[26] The full-system of 5170 atoms is partitioned into two layers defining a boundary at the C−C bond of the Lys296 side chain (i.e., two bonds beyond the C-NH(+) linkage). The QM layer corresponds to a reduced-system with 54 atoms, including 48 atoms of the retinyl chromophore, five atoms of Lys296 ($NH-CH_2$), and a link hydrogen atom that saturates the extra valence of the terminal $-C-H_2$ at the boundary. The MM layer corresponds to the rest of the residues within a 20 Å radius from the chromophore. The remaining environment was subjected to harmonic constraints in order to preserve the overall shape of the protein.[12b,17]

Besides the retynilidene chromophore in rhodopsin (model **1**), several molecular models were also considered to analyze diverse properties (Figure 1): the all-*E*-retinal, which has an aldehyde group instead of the PSB moiety (model **2**);[27] the 11-Z *N*-*tert*-butyl retinylidene imine triflate in solution, which is modeled for computational purposes replacing the *tert*-butyl with a methyl group (model **3**, Figure 1 shows the computational model); the all-*E* *N*-*tert*-butyl retinylidene imine triflate in solution (model **4**);[28] and an all-carbon model obtained from model **1** replacing the nitrogen by a carbon atom and the methyl group bonded to N by a hydrogen atom (model **5**). Model **1** is used for general discussions and calculations of all NMR and electronic properties in this work. Models **1**, **2**, and **4** are used to compute indirect coupling constants in the protein system (**1**) and in isolated systems (**2** and **4**). They are chosen for the availability of experimental NMR indirect coupling constants. Model **3** is a model to test the counterion's sole effect on the electronic properties of the retinylidene chromophore; it is a simplified version of model **4**. Model **5** is an all-carbon model used to analyze how the presence of heteroatoms and other factors in retinal-like compounds affect the conjugation of the polyene conjugated chain. The geometry of **1** was obtained either from QM/MM optimizations, which include the whole protein, or from quantum mechanics geometry optimizations in models immersed in acetonitrile using the B3LYP/6-31G* basis set.

DOI: 10.1021/ct500612n
J. Chem. Theory Comput. 2015, 11, 1206−1219

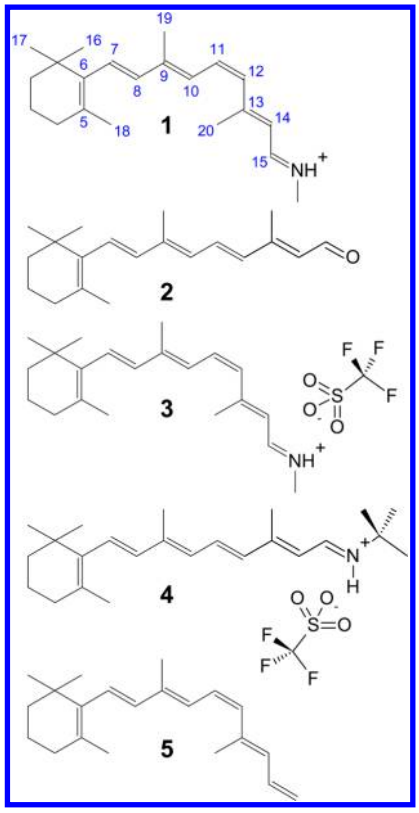

Figure 1. Molecular structures of the retinal compounds. Model **1**: retynilidene chromophore in rhodopsin. Model **2**: all-*E* retinal in solution. Model **3**: 11-Z retinylidene imine triflate in solution (a computational model of the 11-Z *N*-*tert*-butyl retinylidene imine triflate). Model **4**: all-*E* *N*-*tert*-butyl retinylidene imine triflate in solution. Model **5**: an all-carbon model obtained from model **1** replacing the nitrogen by carbon and the methyl group bonded to N by a hydrogen atom.

Models **2** to **5** were optimized in acetonitrile at the B3LYP/6-31G* level. The election of this level of theory in QM and QM/MM models is based on the very good agreement with NMR parameters in a related system.[12b] The solvent is modeled with the polarizable continuum model (PCM) in which the cavity is created via a series of overlapping spheres, a method developed by Tomasi and co-workers.[29]

2.2. Magnetic Shielding. When an external field is applied to a sample, the energy levels of the nuclear spin are modified by the magnetic effect of the surrounding electrons. This effect is called magnetic shielding, and it can be computed from molecular properties alone.

The magnetic shielding can be diamagnetic and paramagnetic. The diamagnetic, Lamb, or ground state shielding arises from the circulation of the electrons at the nucleus, and it reduces the strength of the external magnetic field. Conversely, the paramagnetic term arises from occupied-vacant transitions caused by the external magnetic field. These transitions contribute to unpaired states required for the paramagnetic term. The paramagnetic contribution actually deshields the nuclear spin.

If the electronic wave function is represented by a unideterminantal HF state, the expression of the shielding σ_K for nucleus K according to the Ramsey expression is[30]

$$\sigma_K = \sigma_K^{\mathbf{d}} + \sigma_K^{\mathbf{p}} \tag{1}$$

$$\sigma_K^{\mathbf{d}} = \frac{r_e}{2}\sum_{p=1}^{N}\langle p|\sum_i (\mathbf{r}_{Ki}\cdot\mathbf{r}_{Oi}\mathbf{1} - \mathbf{r}_{Ki}\mathbf{r}_{Oi}^T) r_{Ki}^{-3}|p\rangle \tag{2}$$

$$\sigma_K^{\mathbf{p}} = -4\beta^2 \sum_{p=1}^{N}\sum_{q=N+1}^{\infty} \frac{[\langle p|\sum_i \mathbf{l}_{Ki} r_{Ai}^{-3}|q\rangle\langle q|\sum_i \mathbf{l}_{Oi}\sum_i|p\rangle + c.\ c.]}{(E_{pq} - E_0)} \tag{3}$$

in which $\mathbf{r}_{Ki}$ is the vector position of the electron i from the nucleus K and $\mathbf{r}_{Oi}$ the vector position from center O, $\mathbf{1}$ is the identity operator, $\mathbf{l}$ is the orbital angular momentum operator, N is the number of occupied orbitals, $r_e = e^2/4\pi\varepsilon_0 mc^2$ (where ε_0 is the permittivity of free space, m the mass of the electron, and c the speed of light in a vacuum; r_e = 28.178 ppm Å), $\beta = e\hbar/8\pi\varepsilon_0 mc$ (where β includes the dimensional constant $\hbar$ of the $\mathbf{l}$ operator explicitly; β^2 = 53.682 ppm Å^3 eV), p represents occupied molecular orbitals, q is vacant orbitals, and $E_{pq} - E_0$ is the change of energy from the ground state (E_0) to the singlet excited state (E_{pq}), corresponding to the electronic excitation $p \rightarrow q$. c.c. stands for complex conjugate.

The different magnitudes that appear in the Ramsey equation come from the explicit forms of the vector potential **A**, and the electrostatic potential V. The intensity of the magnetic field does not appear explicitly, due to the very definition of the shielding constant; i.e. if an external magnetic field of unit strength is applied, the magnetic field at the nucleus from electron motions has a component $-\sigma_K$ parallel to the applied field.

The Ramsey expression is included because it emphasizes the physical relation of the involved magnitudes. However, most computational schemes avoid an explicit computation of excited states of the system. Moreover, eqs 2 and 3 refer to a specific common gauge origin (the Ramsey equation shown in eqs 1−3 is with respect to the center O). Other choices of gauge origin will change the individual expressions for σ^{d} and σ^{p}, without formally changing the overall shielding. The reason for this dependence is that the electronic Hamiltonian in the presence of external magnetic fields depends explicitly on the vector potential **A** (through the kinetic term). Although the potential vector depends on the origin of coordinates **O**, the physical field represented by the magnetic induction **B** does not. Except for atoms,[6a] there is not unique and natural election for the gauge origin of the potential vector. In order to guarantee the independence of the gauge origin, the usual approach to evaluate the magnetic properties in molecules is to add complex phase factors to the molecular orbitals (MOs) and atomic orbitals (AOs), explicitly adding to each function a complex phase factor. In the case of the AOs, a spherical harmonic $S_{lm}(\mathbf{r})$ of Gaussian type (GTO) is modified in the following way:

$$\omega_\nu(\mathbf{B}) = \exp[-1/2i\mathbf{B}\times(\mathbf{N}-\mathbf{O})\cdot\mathbf{r}]S_{lm}(\mathbf{r})\exp(-ar^2)] \tag{4}$$

The resulting AOs are known as London atomic orbitals[31] or gauge included atomic orbitals (GIAOs). The GIAO method was applied for the calculation of the shielding tensors, due to a very efficient implementation by Pulay's group,[32] and the general good agreement with experimental data.[12b] ^{13}C NMR shielding tensors are computed at the ONIOM-EE (B3LYP/6-31G*:AMBER)//ONIOM(B3LYP/6-31G*:AMBER) level of theory with the GIAO method,[33] as implemented in Gaussian 03.[32] Chemical shifts are computed with respect to

DOI: 10.1021/ct500612n
J. Chem. Theory Comput. 2015, 11, 1206−1219

trimethylsilane (TMS), consistent with the NMR solid-state experimental data analyzed in this paper.

2.3. Spin−Spin Coupling Computations. Within the framework of the nonrelativistic theory of indirect spin−spin coupling,[34] the interactions between the nuclear spins of different nuclei is transmitted through the surrounding electrons (this is why it is called indirect) by means of two mechanisms: interactions between nuclear and electronic spins (spin−spin interactions) and interactions between nuclear spins and electronic orbital angular momenta (spin-dipolar interactions). The first (spin−spin) mechanism comprises two contributions to the coupling constants: the Fermi-Contact (FC) and the Spin-Dipole (SD) terms. The FC contribution originates from the interaction between nuclear and electronic spins at the nuclear position (the probability to find an electron at the nuclear position has a finite value), while the SD contribution is due to dipole through-space interactions between nuclear and electronic spins. The second (Spin−Orbital, SO) mechanism also has two contributions: Orbital Paramagnetic (OP) and Orbital Diamagnetic (OD). Any indirect coupling constant between K and L nuclei can thus be expressed as a sum of four contributions to the spin−spin coupling:

$$J_{KL} = J_{KL}^{FC} + J_{KL}^{SD} + J_{KL}^{OP} + J_{KL}^{OD} \quad (5)$$

A proper calculation of the FC and SD contributions implies the estimation of the energies corresponding to triplet-excited states and hence requires accounting for electron correlation. This factor is also important but not crucial for the orbital paramagnetic contribution OP, which only involves summation over singlet-excited states.[35] Thus, any *ab initio* calculation of coupling constants should be carried out taking into account a high level of electron correlation. In the present study, the $^{13}C-^{13}C$ coupling constants are calculated allowing electron correlation within the framework of the Coupled Perturbed Density Functional Theory (CPDFT)[36] as implemented in Gaussian 03.[26]

In general, the FC contribution is the most important. However, to achieve quantitative agreement with the experiment, all four contributions must be computed.[36,37] Density functional theory (DFT) was used successfully to evaluate J-coupling constants, in particular J_{CC} and J_{CH} values obtained with hybrid functionals are generally in good agreement with experiments.[38] Among all available density functionals, the hybrid B3LYP[39] (that contains a Hartree−Fock exchange contribution) has been shown to provide good results for spin−spin couplings.[36−38]

The calculation in the framework of density functional theory of $^1J_{CC}$ coupling constants in the rhodopsin chromophore (**1**), and related model compounds all-*E*-retinal (**2**) and all-*E N*-*tert*-butyl retinylidene imine triflate (**4**) is presented, and these results are compared with experimental values.[40] For the pure quantum mechanics systems (**2** and **4**), the same model and DFT functional are used for the J coupling calculations. For the hybrid QM/MM system **1**, the quantum mechanics layer is fully retained while the molecular mechanics region is modeled with a set of point charges at nuclei positions taken from the Amber force field (DFT+AMBER charges).

The calculation of J couplings significantly depends on the quality of the basis set employed.[37,41] Therefore, different basis sets were tested for the J coupling calculations: the 6-31G* basis set, the cc-pVDZ basis set,[42] the cc-pVDZ-sd basis (the cc-pVDZ basis with all the s functions decontracted), the cc-pCVDZ[43] basis set, and the cc-pCVDZ-sd (the cc-pCVDZ basis with all the *s* functions decontracted).

The cc-pCVXZ (X = D or T)[43] basis set is characterized by having an enhanced *s* part through the inclusion of core and core−valence correlation effects to better describe the nuclear region, which is particularly important to compute the FC contribution, while decontracting the *s* functions allows for a greater flexibility, and hence a better description of the wave function at the nucleus position. Note that this is only necessary at the position of the J-coupled nuclei, and hence in this work, decontracted basis sets are restricted to atoms involved in the J-coupling. In this way, an excessive computational cost is avoided, while keeping a reasonable accuracy.

Several tests were run, and it was found that the best agreement with experimental data is achieved with the decontracted cc-pCVDZ-sd applied to the J-coupled nuclei and the cc-pVDZ basis sets to the rest of the molecule. Consequently, this combination was used in all calculations reported herein.

2.4. Electronic-Delocalization Interactions. Resonance Substructures. Electronic-delocalization interactions represent interactions among localized molecular orbitals that give rise to energy stabilization. In the natural bond orbital (NBO) framework,[16] these interactions are represented by delocalizations from high occupancy to low occupancy orbitals that involve a net transference of charge. In the chemical parlance, these interactions are known as hyperconjugative interactions.

Chemical resonance is the representation or modeling of a molecular structure as an average or resonance hybrid between several strictly localized (in terms of single, double, and lone pair orbitals) structures. Each delocalization interaction can be expressed within the framework of the resonance theory as a correction produced by an equilibrium resonant structure. For example, if the atoms A, B, C, and D are bonded as shown in the initial structure (I) of Figure 2, the NBO interaction σ(A−B) → σ^*(C−D) may be interpreted in terms of resonant substructures II and III. Therefore, an intense NBO interaction of the form σ(A−B) → σ^*(C−D) is associated with a resonant structure in which the initial structure I has a reduced weight and the structure II has a high weight. Although there is no fundamental distinction between resonance and delocalization, resonance schemes are closer to the chemical intuition and easier to interpret than the corresponding delocalizations.

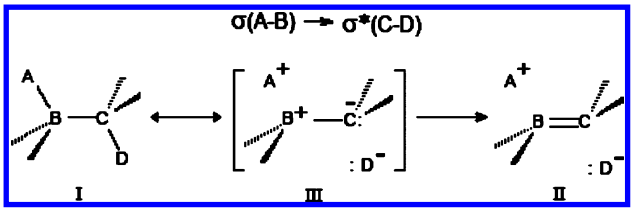

Figure 2. Resonance substructures corresponding to the NBO delocalization σ(A−B) → σ^*(C−D).

The Natural Resonance Theory (NRT)[44] analysis allows calculating accurate weights for different resonance substructures associated with conjugated systems within the NBO framework.

NRT cannot be computed directly within the ONIOM formalism as implemented in Gaussian. To avoid this problem, first the QM/MM wave function was obtained, plugged into an

DOI: 10.1021/ct500612n
J. Chem. Theory Comput. 2015, 11, 1206−1219

isolated chromophore, and then the standard QM computation of NRT proceeded.

2.5. Bond-Length Deviation (BLD) Analysis. Bond length data can be used to gain access to bond length alternation departures from an idealized conjugated chain. Since the bond order is a measure of the relation between σ- and π-electron densities between nuclei, bond lengths have a straightforward relationship with the proportion of π-electron density.

The bond-length deviation (BLD) is a parameter that describes bond alternation departure from idealized models. BLD is the difference between a C−C bond length along the retinylidene chain and a typical value for a C−C bond length with the same bond order. BLD can be expressed as

$$\mathrm{BLD}_{ij} = r_{i,j} - r_0 \tag{6}$$

where $r_{i,j}$ is the bond length between nuclei i and j and r_0 is a typical single- or double-bond length. Depending on the application, r_0 may take typical values (single bond = 1.46 Å, double bond = 1.33 Å)[11] or values from a molecular model, from which the parameter will predict departure from conjugation. BLD is a bond parameter and may be used to analyze conjugation alteration at specified bonds.

2.6. Energy Decomposition Analysis. Intramolecular Natural Energy Decomposition Analysis (INEDA)[45] is a NBO-based methodology[46] that allows the quantification of intramolecular interactions. INEDA partitions the interaction energy into three components:

$$\Delta E = \mathrm{EL} + \mathrm{CORE} + \mathrm{CT} \tag{7}$$

It includes a classical contribution, EL, which arises solely from electrical interactions (both static and induced), and two quantum mechanics contributions: CORE, which accounts for interactions between occupied orbitals ($\sigma \leftrightarrow \sigma$), and charge transfer (CT) interactions, which include occupied-vacant ($\sigma \rightarrow \sigma^*$) delocalizations. The methodology allows the analysis of intramolecular energy influences between different regions of a molecule.

The Coulombic (EL) contribution is the sum of a pure electrostatic term (EL), which corresponds to the interaction between the fragments prior to molecule formation, and a polarization term (POL) that represents the contribution of the charge induced by the presence of the second fragment. The third term is the self-energy (SE), which represents the energy necessary to polarize each fragment:

$$\mathrm{EL} = \mathrm{ES} + \mathrm{POL} + \mathrm{SE} \tag{8}$$

In this paper, the INEDA methodology was extended, currently only available for full QM systems[45] to evaluate interactions within the QM region embedded in a QM/MM model. The extension basically consists of extracting the wave function modified by the presence of the proteinaceous environment and plugging it within the QM-INEDA algorithm implemented in the program GAMESS-US.[47] In practice, GAMESS was fed with a QM/MM wave function from Gausian, without further SCF optimization. The procedure is however not straightforward, as in the INEDA implementation, all wave function optimizations in the workflow are treated equivalently. To avoid this problem, the source code was modified to treat differently the initial wave function, Ψ^{def} and Ψ^{loc} (see ref 45 for more details about the INEDA procedure). Besides, the value of the final energy does not propagate along the program if the SCF cycle does not converge, so the code was also modified to change this behavior. The actual implementation also requires reformatting of the QM/MM wave function from Gaussian style to a format suitable for a GAMESS input file. To extract the pairwise interactions between selected residues and the retynilidene chromophore of rhodopsin, the QM region only includes the two interacting moieties, while the rest of the protein is treated at a MM level.

3. RESULTS

The main goal of this section is to establish the way the protein environment affects the properties of the retinylidene chromophore of rhodopsin. The first step is to determine the contributions of individual residues to the chemical shifts. The best candidates are residues inside the cavity of the retinylidene chromophere in an extended hydrogen-bonding network, which includes two water molecules (Water2a and Water2b) and polar residues Glu-181, Cys-187, Ser-186, and Glu-113.[17] To estimate this contribution, the ^{13}C chemical shifts were computed with the atomic charges of the force field corresponding to the atoms in the side chain of the selected amino acids, and all atoms in the case of water molecules reduced to zero, and this value was subtracted to the magnitude obtained via a standard calculation (Figure 3). The most

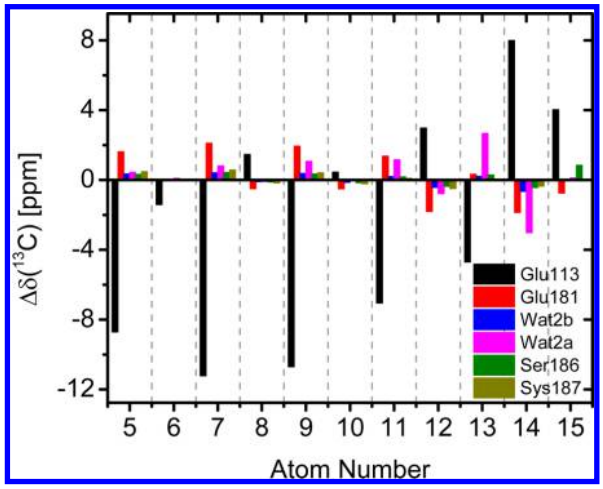

Figure 3. Contribution of selected residues inside the cavity of the retinylidene chromophere to the ^{13}C chemical shifts. See Figure 1 for atom numbering.

important contribution comes from Glu-113, which is directly H-bonded to the N−H of Lys-296. The central role of this residue is manifested in the change of the chemical shifts, as well as in the long-range effect, with notorious effects present deep into the polyene chain.

Evaluation of EL interactions (eq 8) between the above-mentioned residues and retinal will determine the different intensities of the long-range interactions between the residues and retinal. INEDA energies confirm that Glu-113 has the strongest electrical interaction, with the polarization (POL) term having the strongest contribution (Table 1). Glu-113 is hence the residue that most significantly alters the electronic density of the retinylidene chromophore beyond its local environment, and the effect of this residue will be analyzed throughout the rest of this section.

3.1. Bond-Length Deviation (BLD) Analysis. This subsection will be focused on how the electronegative nitrogen atom at the N-terminus, as well as PSB counterions, affect the

DOI: 10.1021/ct500612n
J. Chem. Theory Comput. 2015, 11, 1206−1219

Table 1. Electrical Interaction Energies (in kcal/mol) between Selected Residues and the Retynilidene Chromophore of Rhodopsin

residue	ES	POL	SE	total
Wat2a	−0.41	−2.19	1.10	−1.50
Wat2b	2.79	−0.53	0.27	2.52
Ser-186	−2.36	−4.91	2.51	−4.77
Cys-187	0.45	−0.56	0.29	0.17
Glu-113	−90.34	−33.21	16.80	−106.75
Glu-181	2.17	−0.64	0.32	1.85

conjugation of the π system in the retynilidene chromophore. With that aim, the BLD analysis was computed in four model compounds. The first model is an all-carbon model based on **1**, which lacks electronegative atoms and counterions (model **5**). The other models are model **1** with QM/MM geometry, model **1** optimized in acetonitrile, and model **3**. The all-carbon model allows isolation of the departure of conjugation arising from structural features of retinal (not from electronegative or charged moieties), such as, the cis−trans isomerization, the presence of methyl substituents, and a six-membered ring. The other models introduce the effects of the electronegative N atom and other external groups.

The mere presence of several methyl substituents, and a nonconjugated ring at one end of the chain, makes the bond conjugation of the all-carbon polyene chain depart from an idealized conjugated linear hydrocarbon of the same length (1,3,5,7,9,11-dodecahexaene; Figure 4a). Comparison of bond lengths in model **5** with 1,3,5,7,9,11-dodecahexaene, both optimized at the same level of theory, shows that **5** has an extended disruption of conjugation along the chain. This

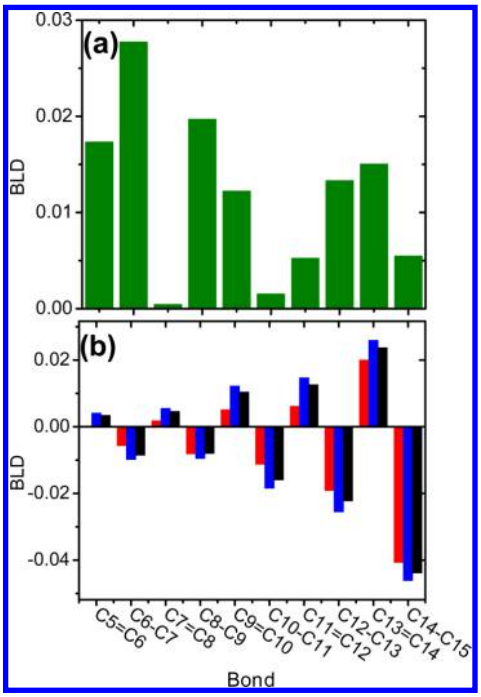

Figure 4. Bond-length deviations (BLD). (a) All-carbon retinal model with respect to ideal bond-length distances in conjugated systems and (b) the following models with respect to an all-carbon retinal model: blue bars, model **1** optimized in acetonitrile; black bars, model **3**; red bars, model **1** with QM/MM geometry. See Figure 1 for atom numbering.

disruption is observed as an increase of bond lengths compared with the idealized conjugated hydrocarbon. As expected, the major effects are at the ring end, observed as elongations of the C(5)═C(6) and C(6)—C(7) bonds, and in the vicinity of the methyl positions (C(8)—C(9) and C(9)═C(10), and C(12)—C(13) and C(13)═C(14) bonds). Minor bond-length increases are also observed at the *cis* bond C(11)═C(12), and in the C(14)—C(15) bond at the PSB terminus (Figure 4a). The presence of methyl groups distorts the planar structure of retinal and hence alters conjugation, such as in the case of the methyl at C(13), which causes the deviation from planarity of the C(10)−C(11)═C(12)−C(13) moiety.[48]

Comparison of an isolated retinal model (model **1** optimized in solvent) and the all-carbon model shows that the introduction of a nitrogen atom increases the conjugation of the all-carbon model, which is more noticeable close to the PSB end, with a monotonic decrease toward the ring end (Figure 4b, blue bars).

The addition of a counteranion (model **3**) decreases conjugation with respect to retinal in the solvent (Figure 4b, black bars), and inclusion of the whole protein decreases conjugation even further (Figure 4b, red bars). This confirms that the effect of residues other than Glu-113 also produces a decrease of conjugation compared with retinal in solution. In a similar analysis based on the 2.6 Å resolution retinal structure with PDB accession code 1L9H,[19] a conjugation defect was found in the region of the C(12)−C(13) bond, close to the structural water molecule between Glu-181 and Ser-186 (Wat2a),[11] which could not be confirmed. This dissimilarity may arise from the use of different structural models. My model is based on a different X-ray structure (PDB accession code 1F88). In addition, this structure was further optimized at the QM/MM level and validated by ^{13}C and ^{1}H NMR data, which gives an improved structural model over the initial XRD structure. This interpretation is reinforced taking into account that noncharged residues do not affect significantly the electronic structure of the chromophore (Table 1) and effectively do not alter significantly the conjugation of the chain (compare black and red bars in Figure 4).

In summary, the distinctive structural features of the retynilidene chromophore (a ring, methyl groups, isomerization) decrease conjugation with respect to single and double bond distances from an ideal linear conjugated system. Conversely, switching a carbon to nitrogen increases conjugation. Moreover, the addition of a PSB counteranion decreases the bond conjugation with respect to the former, and inclusion of the effect of the rest of the protein decreases the conjugation even further.

3.2. Electronic Density. The overall polarization effect that the protein background exerts over the charge distribution can be directly assessed calculating the difference of the electronic charge density of the retinylidene chromophore in the presence and absence of the protein environment (Figure 5). The QM/MM density cannot be compared directly to the QM density, as both formalisms use the basis sets differently. To avoid this problem, the QM/MM wave function was obtained and plugged into an isolated chromophore, and then the charge density was computed in an equivalent way to that in the QM approach. One of the most pronounced effects is the accumulation of electronic (negative) charge density over odd-numbered nuclei of the polyene chain, with increasing intensity in the order 13, 11, 9, 7, and 5. In addition, the protein environment induces a decrease of electronic density over the

DOI: 10.1021/ct500612n
J. Chem. Theory Comput. 2015, 11, 1206−1219

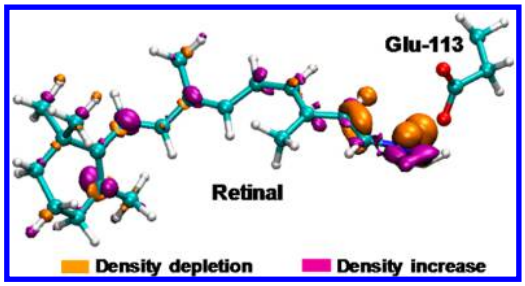

Figure 5. Electronic charge density difference between the chromophore in the presence and absence of the protein environment. Orange isosurfaces indicate depletion of electronic charge, while purple surfaces indicate negative (electronic) charge accumulation. Note that there is a net increase of electronic density toward the ring end, while a net positive charge is accumulated on the imine terminus side.

$C_{14}-C_{15}$ bond, with an isosurface shape that clearly resembles a π-orbital. This depletion is due to the anticooperative effect of the Glu-113 anion on the $\pi(C(13)=C(14)) \rightarrow \pi^*(C(15)=N)$ interaction, which reduces the π character of the electron density on the C(14)−C(15) bond (see section 3.3 for further details).

The difference of ESP charges in the presence and absence of an external electric field generated by an ideal point charge of −1 au at 1.5 Å of the imine proton of **1** (with ONIOM geometry) was also computed. The resulting effect is consistent with the electronic density findings, with accumulation of negative charge toward the ring end, and an increase of positive charge on the iminine side, which corresponds to a standard polarization pattern (Figure 6). Interestingly, odd-numbered nuclei have the greater change, which suggests that the polyene ring redistributes charge via a conjugated mechanism.

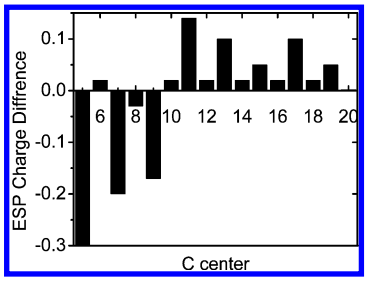

Figure 6. Difference of ESP atomic changes, after the addition of a point charge of magnitude −1 au at 1.5 Å from the imide proton of the PSB. See Figure 1 for atom numbering.

3.3. Natural Resonance Theory (NRT) Analysis. In this section, an analysis of the role of different external interactions on the weight of resonance forms of the conjugated chain is presented using the NRT methodology presented in section 2.4. The mechanisms of influence of Glu-113 on the retinal are analyzed using a modified QM/MM model **1**, in which Glu-113 is taken from the MM layer and included in the QM layer, without further optimization (**1**+Glu). This way, the resonance substructures will incorporate delocalizations between the glutamate and retinal. As this work focuses on retinal properties, resonance substructures will be grouped together with different resonance substructures associated with the glutamate group, provided they share the same resonance substructure in the polyene chain. The most notable finding is that the presence of Glu-113 creates a marked reduction of conjugation. This reduction manifests in the increase of weight of a single substructure, instead of several substructures having similar weights. As shown in Figure 7, substructure I manifests a

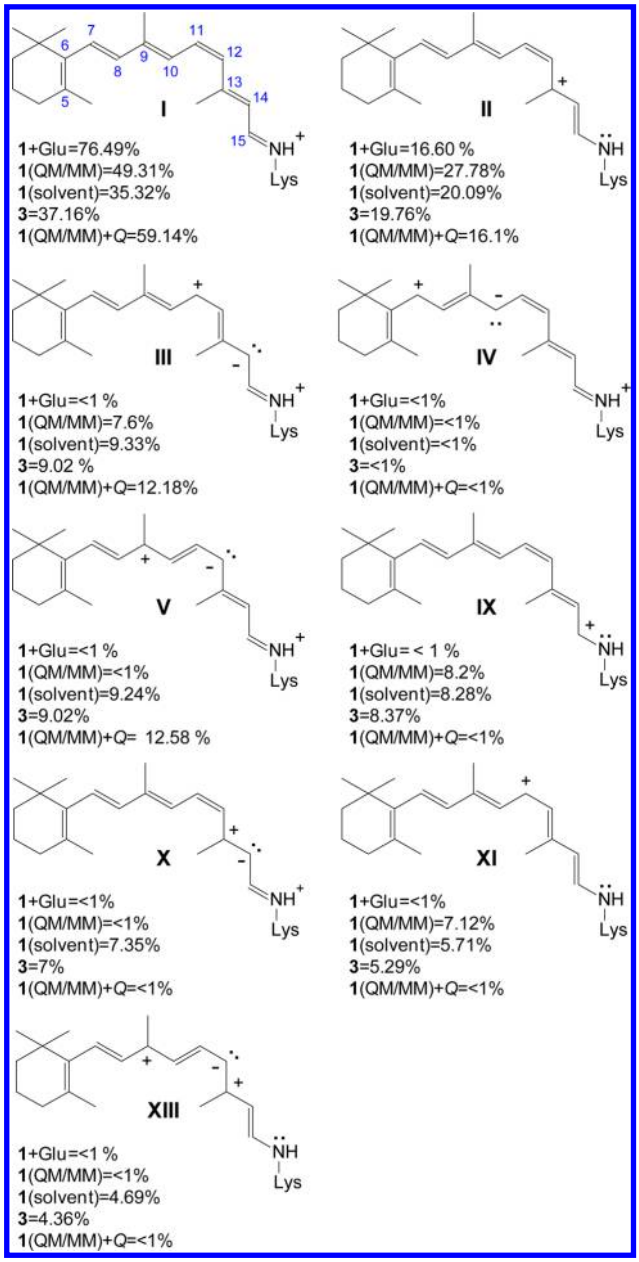

Figure 7. Weighting factors of natural resonance substructures (NRTs) in the retinylidene chromophore. Several scenarios were explored which include **1**(QM/MM), QM/MM structure of model **1** with NRT calculation in a vacuum; **1**+Glu, model **1** plus Glu-113 in the QM region of the ONIOM model with NRT calculation in the protein; **1**(in solvent), model **1** reoptimized in solvent with NRT calculation in solvent; **3**, model **3** with NRT calculation in solvent; and **1**(QM/MM)+Q, model **1** with ONIOM geometry in the presence of a −1 au point charge, with NRT calculation in a vacuum.

relative weighting increase in going from 49.31% without Glu (**1**(QM/MM)) to 76.49% with Glu-113 (**1**+Glu), while substructure II reduces its weight from 27.78% without Glu to 16.60% with Glu. Resonance II is associated with the $\pi(C(13)=C(14)) \rightarrow \pi^*(C(15)-N)$ delocalization, and its decrease is consistent with the depletion of charge with "π

DOI: 10.1021/ct500612n
J. Chem. Theory Comput. 2015, 11, 1206−1219

symmetry" between C_{14} and C_{15}, depicted in the electronic density map (Figure 5). Shifting of the resonance equilibrium to substructures with positive ions localized on the imine terminus promotes a polarization pattern, with reduction of negative charge density closer to the counteranion, and a concomitant increase of negative density at the opposite side of the chain. A low resonance weight corresponding to the maximum delocalization from a carboxylate oxygen lone pair of Glu-113 to the retinal $n(O) \rightarrow \sigma^*(N-H)$ (6.91%, not shown in Figure 7) shows that orbital delocalization is not the most important influence of the glutamate to the retinal. Instead, the main influence is an electrostatic effect on the resonance equilibrium.

To isolate the effect of the counteranion alone, without the protein, resonant weighting factors of two related models with and without a counteranion were computed, i.e. **3** and **1**(in solvent), respectively. These two models are comparable as they are both optimized in solvent. This comparison confirms the observed tendency to reduce conjugation with the addition of the counteranion (higher relative weight of substructure I), with a lesser contribution of resonant structures with positive charges on odd-numbered nuclei (Figure 7). Due to the reduction of polarization caused by the solvent, weighting factor differences in this comparison are smaller than in equivalent moieties in the protein (compare **1**(QM/MM) and **1**+Glu).

In an attempt to isolate the electrostatic effect from delocalizations, a last test was considered with a background point charge of magnitude −1 au at 1.5 Å from the imine proton (**1**(QM/MM)+*Q*). The external charge produces a marked increase of the weight of substructure I, which has a formal positive ion on N, from 49.31% in **1**(QM/MM) to 59.14% in **1**(QM/MM)+*Q*, and also an overall small increase of susbstructures II, III, and beyond, from 27.78% in **1**(QM/MM) to 16.10%, 12.58%, etc. in **1**(QM/MM)+*Q* (Figure 7). The background charge therefore decreases the conjugation and enhances the weight of resonant structures with partial positive charges closer to the negative charge, compared with the retinal without counterion. It can hence be concluded that the charge alone can reproduce most of the features of the effect of the external environment on the resonance properties of retinal. However, as pointed out when analyzing BLDs, the effect of the whole protein is even more intense, due to the effect of the other amino acids, which tend to reduce conjugation even further.

In summary, the effect of the protein on the resonance equilibrium, which mostly follows the electrostatic effect of Glu113, creates a reduction of conjugation, with accumulation of negative density at odd-numbered carbon centers with increasing intensity from the PSB to the ring end. This result is consistent with the more simplistic BLD analysis described in section 3.1, based on geometries of optimized models alone.

3.4. ^{13}C Chemical Shifts. There is a high correlation between calculated and experimental ^{13}C chemical shifts of the 11-*cis*-retinyl chromophore (Figure 8),[11,12b] which reveals that the chosen combination of geometry and level of theory closely reproduces the experimental data. To isolate the effect of the protein environment over the chemical shifts, the difference of the ^{13}C NMR chemical shifts of carbon nuclei in the presence and absence of the protein environment were computed (Figure 9). The depicted pattern shows an alternating behavior that affects more markedly the odd numbered carbons. This

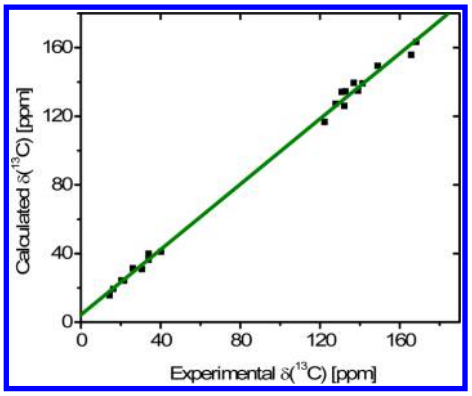

Figure 8. Correlation between experimental[12a,c] and calculated ^{13}C chemical shifts of the retinylidene chromophore of rhodopsin calculated at the ONIOM Electronic-Embedding ONIOM-EE (B3LYP/6-31G*:AMBER) level of theory. ρ = 0.999, slope =0.952, N = 20.

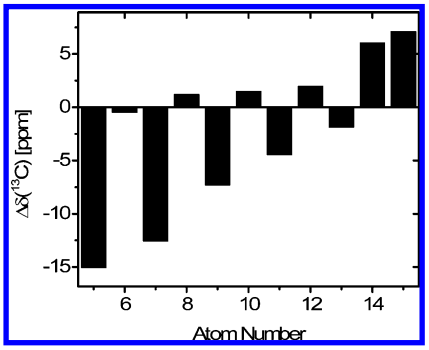

Figure 9. Effect of the protein environment over the magnetic shieldings, estimated as the difference of ^{13}C NMR chemical shifts of carbon nuclei calculated including the protein environment (via the ONIOM-EE method) and the chromophore in a vacuum. See Figure 1 for atom numbering.

effect is also modulated in amplitude, with increasing intensity in going from C(13) to C(5).

The presence of methyl substituents is consistent with an increase of the shieldings at those centers. The most shielded nucleus is C(13) due to being a quaternary carbon, and its proximity to the NH^+ shielding center (Table 2).

As mentioned at the beginning of this section, Glu-113 is responsible for alternation (odd-numbered nuclei), and modulation of the NMR shieldings with increasing intensity from C(13) to C(5) (Figure 3). The intensity of the modulation is consistent with an electrostatic repulsion exerted by the counteranion charge, which shifts negative charge toward the inner side of the polyene chain, thus creating polarization of the chain with an increase of negative charge (shielding) toward the ring end, and positive charge on the imine terminus side. To test this hypothesis further, I experimented adding an ideal point charge of magnitude −1 au at 1.5 Å from the imine proton to the PSB model isolated from the protein (geometry from the QM/MM optimization, with no solvent). The results are consistent with the above-mentioned analysis and indeed show that they have a comparable magnitude (Figure 10).

Although the ONIOM-EE methodology allows repolarization of the QM layer due to the MM layer, electron delocalizations between the Glu and the retinal are not fully included between layers. As the quantum mechanics treatment

DOI: 10.1021/ct500612n
J. Chem. Theory Comput. 2015, 11, 1206−1219

Table 2. Experimental and Calculated Chemical Shifts Relative to TMS of the Retynilidene Chromophore of Rhodopsin

C	^{13}C chemical shift [ppm]	
	experimental	calculated[c]
C(1)	34.0[a]	39.06
C(2)	40.3[a]	40.08
C(3)	20.3[a]	23.45
C(4)	34.0[a]	35.52
C(5)	130.3[b]	133.43
C(6)	137.7[b]	138.77
C(7)	132.3[b]	134.21
C(8)	139.2[b]	133.78
C(9)	148.5[b]	149.09
C(10)	127.8[b]	126.11
C(11)	141.6[b]	138.55
C(12)	132.1[b]	124.89
C(13)	168.9[b]	162.18
C(14)	121.2[b]	115.60
C(15)	165.4[b]	153.49
C(16)	30.6[a]	30.60
C(17)	26.1[a]	29.96
C(18)	21.7[a]	23.28
C(19)	14.4[a]	14.73
C(20)	16.3[a]	18.42

[a]Data from ref 12c. [b]Data from ref 12a. [c]Calculated at the ONIOM Electronic-Embedding ONIOM-EE (B3LYP/6-31G*:AMBER) level of theory.

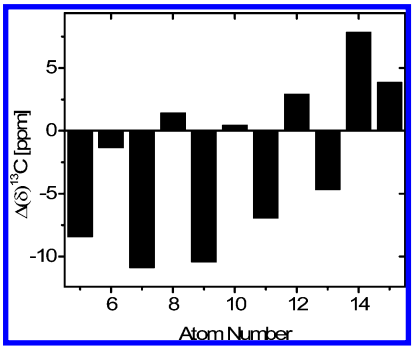

Figure 10. ^{13}C chemical shift differences with and without the addition of a point charge of magnitude −1 au at 1.5 Å from the imide proton of the PSB. See Figure 1 for atom numbering.

enables electron delocalization features, the ^{13}C shielding tensors were recalculated in a model that includes Glu-113 as part of the QM layer in the QM/MM framework. This inclusion produces no significant changes to the magnetic properties, consistently with the NRT analysis.

The combined analysis of inclusion/exclusion of the protein, zero AMBER charges, the addition of a test-point charge, inclusion/exclusion of Glu-113 within the quantum mechanics layer, and INEDA analysis indicates that the counteranion is the main influence of the magnetic shieldings and is exerting its influence largely through an inductive mechanism carried out by the conjugated system.

3.5. ^{13}C−^{13}C *J*-Couplings in the Rhodopsin Chromophore. $^{1}J_{CC}$ coupling-constant experiments suggest that the effect of the protein may not reach that far into the polyene chain, compared with chemical shifts. To determine the origin of this inconsistency, the relation between coupling constants and electronic properties was analyzed. Figures 11 and 12 show a comparison between calculated and experimental $^{1}J_{CC}$

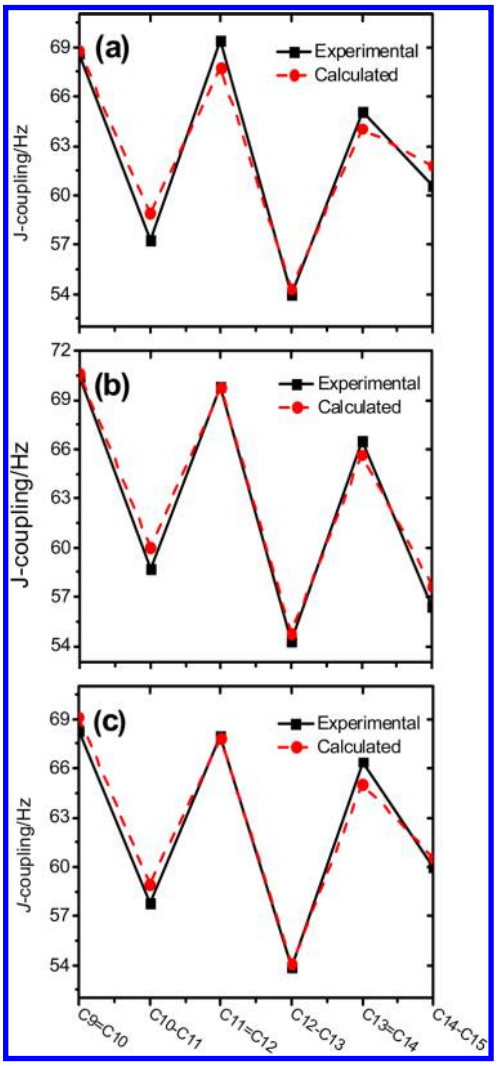

Figure 11. Calculated and experimental[13] $^{1}J_{CC}$ coupling constants corresponding to selected ^{13}C−^{13}C bonds of (a) retynilidene chromophore of rhodopsin **1**, (b) all-*E* retinal in solution **2**, and (c) all-*E N*-*tert*-butyl retinylidene imine triflate in solution **4**. See Figure 1 for atom numbering.

coupling constants for compounds **1**, **2**, and **4**. Both calculated and experimental values for the three model compounds agree within experimental uncertainties showing again that the QM/MM model closely mimics the intrinsic electronic properties of the experimental systems.

The only point that differs significantly between the three models is the value of $^{1}J_{CC}$(C(14)−C(15)), which is smaller in retinal (**2**), compared with rhodopsin (**1**) and the PSB model compound **4**. The enhancement in **1** and **4** can be attributed to the nearby PSB counteranion, which exerts a local influence. The *J*-couplings therefore provide no indication that the protein environment significantly perturbs the electronic structure of the conjugated system, apart from the localized effects of the PSB at the imine terminus side.

3.6. C−C Bond Distance and $^{1}J^{13}$C−^{13}C Correlations. A low correlation (ρ = 0.975) is obtained between the spin coupling constants and bond lengths (Figure 13). The internuclear distance is mainly dependent on the $\sigma-\pi$ character

DOI: 10.1021/ct500612n
J. Chem. Theory Comput. 2015, 11, 1206−1219

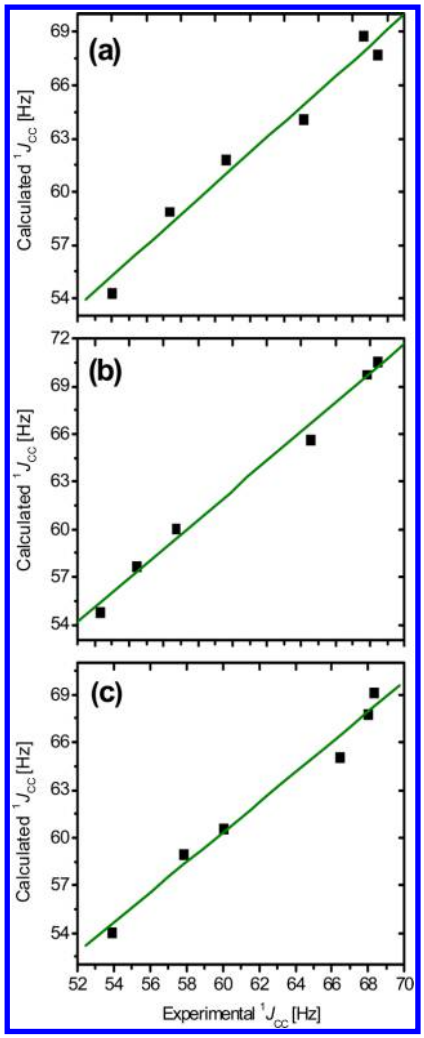

Figure 12. Correlation between experimental[13] and calculated ^1J $^{13}C-^{13}C$ spin−spin coupling constants of (a) retynilidene chromophore of rhodopsin **1** (ρ = 0.986), (b) all-*E* retinal in solution **2** (ρ = 0.996), and (c) all-*E N*-*tert*-butyl retinylidene imine triflate in solution **4** (ρ = 0.990).

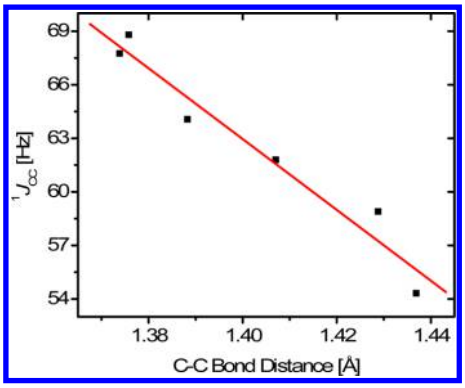

Figure 13. Correlation between QM/MM $^1J_{CC}$ coupling constants and C−C bond lengths. ρ = 0.975, N = 6.

of the bond, which is determined by the valence orbitals. The spin coupling constants, on the other hand, are dependent on the electron density at the nuclear position (core orbitals of s-type) through the Fermi contact term.[49]

3.7. Relation with Previous Works. Other groups have applied DFT approaches to analyze the ground state of the chromophore in rhodopsin. Calculations by Touw et al. in protonated models (similar to model **1** optimized in acetonitrile)[50] reveal a polaronic conjugation defect in the Schiff base region. They found that the C(14)−C(15) bond has enhanced double bond character, while the C(13)═C(14) and C(15)═N bonds have reduced double bond character, in accordance with the BLD analysis (Figure 4b, black bars). These authors also found that the PSB counterion charge is strongly delocalized in the region around the polyene chain of the chromophore, in accordance with the present study (Figure 6). Buda et al. also use DFT to study retinylidene iminium salts, and they found that the amplitude of the bond length alternation between single and double carbon bonds is strongly reduced in the vicinity of the protonated Schiff base nitrogen,[51] in accordance with these results (Figure 4b). An NMR analysis based on molecular dynamics simulations in a QM/MM framework by the Sebastiani group reaches the conclusion that both ^{13}C and the ^1H NMR chemical shifts are rather insensitive to the protonation state of Glu181.[24] This result implies that the electrostatic influence of an ionizable amino acid side chain located in the vicinity of the retinal has small effects on the chemical shifts, in accordance with my observations.

4. DISCUSSION

The addition of a counteranion at the PSB side of the polyene chain induces polarization, which accumulates electronic density on the opposite side of the chain. In resonance parlance, selection of resonant structures with positive ions closer to the counteranion means resonance substructures with negative ions toward the ring end. Those resonance substructures benefit more negative electron density around carbon centers close to the terminal ring, in accordance with ESP and ^{13}C chemical shifts. This effect produces more intense shieldings at lower-numbered carbons (Figure 9). The effect of the whole protein environment on the analyzed properties is mostly consistent with the sole effect of Glu-113, which means that other protein residues and water molecules in the first coordination shell of the chromophore have lesser effects on the magnetic shielding. This result is consistent with previous studies,[12b] and with the analysis of interaction energies (INEDA).

With respect to spin coupling constants, the indirect spin coupling between ^{13}C centers is dominated by the Fermi contact term.[49b] As a result, they will depend on the product of the core s electron densities at the coupled nuclei (eq 8). Molecular orbital calculations carried out in order to separate σ- and π-transmitted components of the Fermi contact, spin-dipolar, and orbital terms of $^{13}C-^{13}C$ coupling constants in several unsaturated hydrocarbons[52] showed that the FC interaction is mostly transmitted through the σ system. On the other hand, the SO interaction requires the π system for transmitting the information. The SD interaction, although having a similar behavior to the SO component, has a small σ contribution as well. The dominant contribution to the one-bond couplings is by far the FC term,[52b,53] which means that the coupling interactions are mainly transmitted through the σ system.

A negative counteranion charge affects π orbitals along the chromophore conjugated chain, as confirmed by the BLD diagrams and NRT analysis, while only affecting σ bonds significantly close to the perturbation. Because ^{13}C magnetic shieldings are predominantly dependent on valence π orbitals, chemical shift values are largely influenced by the perturbation

DOI: 10.1021/ct500612n
J. Chem. Theory Comput. 2015, 11, 1206−1219

of the conjugation, affecting their magnitudes deep into the conjugated chain, as observed experimentally.[12c] Conversely, external effects on the coupling constants are mainly transmitted through the σ orbitals, which are less affected by conjugation, and hence their values are less prone to be altered penetrating deep into the hydrocarbon chain.[13] Thus, the apparent contradiction between experimental findings based on chemical shifts (deep penetration)[12c] and one-bond *J*-couplings (localized effects of the PSB at the chain terminus)[13] is in fact a consequence of different properties responding differently to the same external perturbation.

How may the discussed ground state results affect the photochemical properties of rhodopsin? It can be hypothesized that the selective photoisomerization at C(11)=C(12), which occurs in rhodopsins, can be assisted by the following effects of the environment on the electronic structure of the ground state of the PSB:

1. The C(11)=C(12) double bond elongates along the cis−trans photoisomerization path, which is triggered by excitation to the spectroscopic S1 state,[54] and this stretch can be considered as a manifestation of the increase of conjugation. In accordance with the present findings, the presence of the counterion decreases bond conjugation in the ground state, which also involves a decrease of the C(11)=C(12) double-bond length. Since conjugation generally moves the absorption maxima to longer wavelengths,[55] the decrease of conjugation can be associated with a hypsochromic shift. In addition, the effect of the rest of the protein reduces the conjugation even further (Figure 4b), adding an extra contribution to a blue opsin shift.

2. The absorption spectrum of rhodopsin represents to a large extent the difference in energy levels between the ground state (S_0) and the first excited state (S_1). So any factors that affect any of these levels are expected to affect the absorption maxima λ_{max} value. As the counterion neutralizes the positive charge of retinal, it is expected to stabilize the ground state of the chromophore and hence reinforces the contribution to a blue shift.

3. In the ground state, solid-state NMR[48a,56] and resonance Raman spectroscopy[48c,d] show a distortion from planarity of the C(10)−C(11)=C(12)−C(13) dihedral angle, which is also observed in the X-ray structure. In the QM/MM model, this torsional distortion is also reproduced with a value of about 13°. This twist suggests a preparation of the nuclear positions along the C(11)=C(12) photoisomerization trajectory.

4. According to the QM/MM findings, the opsin effect also involves accumulation of charge on C(11) (Figure 6). Shifting of the charge density from the imine terminus side to the isomerizing moiety and beyond rearranges the charge in accordance with the charge redistribution along the photoisomerization path identified by CASSCF and CASPT2 studies,[15e,57] in which the positive charge initially located at the imine terminus side migrates, localizing on the isomerizing moiety.

5. SUMMARY AND CONCLUSIONS

From a methodological point of view, the statistical analysis carried out in terms of calculated and experimental NMR data (^{13}C chemical shifts and spin−spin coupling constants) gives experimental support to the ONIOM(DFT:AMBER)-EE structure of the 11-*cis*-retinylidene chromophere of the rhodopsin optimized structure.[17] It also shows that the calculation of chemical shifts using the DFT/GIAO method within the ONIOM-EE hybrid approach with the B3LYP functional and 6-31G* basis set and the calculation of coupling constants using a combination of DFT with AMBER charges approach, with the B3LYP functional, and the decontracted cc-pCVDZ-sd basis set applied to the *J*-coupled nuclei and the cc-pVDZ basis sets to the rest of the molecule are appropriate methods to evaluate NMR parameters in biological systems.

The opsin effect on the retinylidene chromophere can be interpreted as a readjustment of the weighting factors of the resonance substructures corresponding to the conjugated chain of the chromophere. The major effect accounts for the inductive effect of Glu-113 and involves an increase of electronic charge over the protonated Schiff base and a depletion of charge around the C(13)=C(14) bond. The mechanism in terms of stereoelectronic interactions mainly involves a decrease of the strength of the π(C(13)=C(14)) → π^*(C(15)−N) interaction, which in turn alters the relative weighting factors of the possible resonance substructures of the conjugated chain. The change of the weighting factors also gives a rationalization of the alternating effect over the magnitudes of the ^{13}C chemical shifts when comparing the retinylidene chromophere in the presence and absence of the protein environment. On the other hand, being that the indirect coupling constants are mainly dependent on the charge density at the nuclei position, they are less prone to follow the modulation of charge transmitted through π-valence orbitals. In this way, the counteranion effect is restricted to the vicinity of the perturbation, preventing the observation of significant differences of spin coupling constants from different PSBs and all-*E*-retinal.

The other important aspect highlighted in the manuscript is the central role of the Glu-113 counterion compared with the other residues in the retinylidene chromophere cavity. This property was observed both at the electronic level as well as with NMR parameters. The main reason for this preponderance is that the Glu-113 carries a formal negative charge, while all other residues in the chromophore cavity are neutral. However, the results on the present manuscript do not rule out other possible minor effects on the retinylidene chromophere caused by nearby residues in the cavity.

The reported results are particularly relevant to advancing our understanding of the role of the protein environment in determining the electronic properties in the vicinity of the isomerization site of prototypical G-protein-coupled receptors.

AUTHOR INFORMATION

Corresponding Author

*E-mail: e.sproviero@usciences.edu.

Notes

The authors declare no competing financial interest.

ACKNOWLEDGMENTS

The author thanks the two reviewers of the manuscript for their valuable comments, the support of the members of the Department of Chemistry & Biochemistry, USciences, and support from the National Science Foundation (NSF CHE-1229564). The author also thanks Professor Vojislava Torbica-Pophristic for reading the manuscript and for helpful comments.

DOI: 10.1021/ct500612n
J. Chem. Theory Comput. 2015, 11, 1206−1219

ABBREVIATIONS

PSB, protonated Schiff base; GPCR, G-protein-coupled receptors; NMR, nuclear magnetic resonance; QM, quantum mechanics; QM/MM, quantum mechanics/molecular mechanics; DFT, density functional theory; NBO, natural bond orbitals; NRT, natural resonance theory; INEDA, intramolecular natural energy decomposition analysis; GIAO, gauge independent atomic orbital; CPDFT, Coupled Perturbed Density Functional Theory; FC, Fermi contact; SO, spin orbital

REFERENCES

(1) Lagerstrom, M. C.; Schioth, H. B. Structural diversity of G protein-coupled receptors and significance for drug discovery. *Nat. Rev. Drug Discovery* **2008**, *7*, 339−357.

(2) (a) Sakmar, T.; Franke, R.; Khorana, H. Glutamic acid-113 serves as the retinylidene Schiff-base counterion in bovine rhodopsin. *Proc. Natl. Acad. Sci. U.S.A.* **1989**, *86*, 8309−8313. (b) Zhukovsky, E.; Oprian, D. Effect of carboxylic-acid side-chains on the absorption maximum of visual pigments. *Science* **1989**, *246*, 928−930.

(3) von Lintig, J.; Kiser, P. D.; Golczak, M.; Palczewski, K. The biochemical and structural basis for trans-to-cis isomerization of retinoids in the chemistry of vision. *Trends Biochem. Sci.* **2010**, *35*, 400−410.

(4) (a) Andrec, M.; Montelione, G. T.; Levy, R. M. Estimation of dynamic parameters from NMR relaxation data using the Lipari-Szabo model-free approach and Bayesian statistical methods. *J. Magn. Reson.* **1999**, *139*, 408−421. (b) Mandel, A. M.; Akke, M.; Palmer, A. G. Backbone Dynamics of Escherichia-Coli Ribonuclease Hi - Correlations with Structure and Function in an Active Enzyme. *J. Mol. Biol.* **1995**, *246*, 144−163. (c) Macek, P.; Novak, P.; Zidek, L.; Sklenar, V. Backbone motions of free and pheromone-bound major urinary protein I studied by molecular dynamics simulation. *J. Phys. Chem. B* **2007**, *111*, 5731−5739.

(5) Luchinat, C.; Soriano, A.; DjinovicCarugo, K.; Saraste, M.; Malmstrom, B. G.; Bertini, I. Electronic and geometric structure of the Cu-A site studied by H-1 NMR in a soluble domain of cytochrome c oxidase from Paracoccus denitrificans. *J. Am. Chem. Soc.* **1997**, *119*, 11023−11027.

(6) (a) Helgaker, T.; Jaszunski, M.; Ruud, K. Ab initio methods for the calculation of NMR shielding and indirect spin-spin coupling constants. *Chem. Rev.* **1999**, *99*, 293−352. (b) deDios, A. C. Ab initio calculations of the NMR chemical shift. *Prog. Nucl. Magn. Reson. Spectrosc.* **1996**, *29*, 229−278. (c) Fukui, H. Theory and calculation of nuclear shielding constants. *Prog. Nucl. Magn. Reson. Spectrosc.* **1997**, *31*, 317−342.

(7) Grutzner, J. B. In *Recents Advances in NMR Spectroscopy*; Lambert, J. B.; Rittner, R., Eds.; Norell Press: Landisvile, NJ, 1987; p 28.

(8) Richter, W. E.; Pontes, R. M.; Abiko, L. A.; Gauze, G. F.; Basso, E. A. Computation of 3JHH coupling constants with a combination of density functional theory and semiempirical calculations. Application to complex molecules. *Comp. Theor. Chem.* **2012**, *1001*, 7−14.

(9) (a) Helgaker, T.; Lutnaes, O. B.; Jaszunski, M. Density-functional and coupled-cluster singles-and-doubles calculations of the nuclear shielding and indirect nuclear spin-spin coupling constants of o-benzyne. *J. Chem. Theory Comput.* **2007**, *3*, 86−94. (b) Di Micco, S.; Chini, M. G.; Riccio, R.; Bifulco, G. Quantum Mechanical Calculation of NMR Parameters in the Stereostructural Determination of Natural Products. *Eur. J. Org. Chem.* **2010**, *2010*, 1411−1434.

(10) (a) Karplus, M. Contact Electron-Spin Coupling of Nuclear Magnetic Moments. *J. Chem. Phys.* **1959**, *30*, 11−15. (b) Karplus, M. Vicinal Proton Coupling in Nuclear Magnetic Resonance. *J. Am. Chem. Soc.* **1963**, *85*, 2870−&. (c) Juranic, N.; Ilich, P. K.; Macura, S. Hydrogen-Bonding Networks in Proteins as Revealed by the Amide (1)J(Nc′) Coupling-Constant. *J. Am. Chem. Soc.* **1995**, *117*, 405−410.

(11) Carravetta, M.; Zhao, X.; Johannessen, O. G.; Lai, W. C.; Verhoeven, M. A.; Bovee-Geurts, P. H. M.; Verdegem, P. J. E.; Kiihne, S.; Luthman, H.; de Groot, H. J. M.; deGrip, W. J.; Lugtenburg, J.; Levitt, M. H. Protein-Induced Bonding Perturbation of the Rhodopsin Chromophore Detected by Double-Quantum Solid-State NMR. *J. Am. Chem. Soc.* **2004**, *126*, 3948−3953.

(12) (a) Smith, S. O.; Palings, I.; Miley, M. E.; Courtin, J.; de Groot, H.; Lugtenburg, J.; Mathies, R. A.; Griffin, R. G. *Biochemistry* **1990**, *29*, 8158−8164. (b) Gascon, J. A.; Sproviero, E. M.; Batista, V. S. QM/MM study of the NMR spectroscopy of the retinyl chromophore in visual rhodopsin. *J. Chem. Theory Comput.* **2005**, *1*, 674−685. (c) Creemers, A. F. L.; Kiihne, S.; Bovee-Geurts, P. H. M.; DeGrip, W. J.; Lugtenburg, J.; de Groot, H. J. M. 1H and 13C MAS NMR evidence for pronounced ligand−protein interactions involving the ionone ring of the retinylidene chromophore in rhodopsin. *Proc. Natl. Acad. Sci. U.S.A.* **2002**, *99*, 9101−9106.

(13) Lai, W. C.; McLean, N.; Gansmuller, A.; Verhoeven, M. A.; Antonioli, G. C.; Carravetta, M.; Duma, L.; Bovee-Geurts, P. H. M.; Johannessen, O. G.; de Groot, H. J. M.; Lugtenburg, J.; Emsley, L.; Brown, S. P.; Brown, R. C. D.; DeGrip, W. J.; Levitt, M. H. Accurate measurements of C-13-C-13 J-couplings in the rhodopsin chromophore by double-quantum solid-state NMR spectroscopy. *J. Am. Chem. Soc.* **2006**, *128*, 3878−3879.

(14) Okada, T.; Sugihara, M.; Bondar, A. N.; Elstner, M.; Entel, P.; Buss, V. The retinal conformation and its environment in rhodopsin in light of a new 2.2 angstrom crystal structure. *J. Mol. Biol.* **2004**, *342*, 571−583.

(15) (a) Rajamani, R.; Gao, J. Combined QM/MM study of the opsin shift in bacteriorhodopsin. *J. Comput. Chem.* **2002**, *23*, 96−105. (b) Yamada, A.; Kakitani, T.; Yamamoto, S.; Yamato, T. A computational study on the stability of the protonated Schiff base of retinal in rhodopsin. *Chem. Phys. Lett.* **2002**, *366*, 670−675. (c) Ferré, N.; Olivucci, M. Probing the Rhodopsin Cavity with Reduced Retinal Models at the CASPT2//CASSCF/AMBER Level of Theory. *J. Am. Chem. Soc.* **2003**, *125*, 6868−6869. (d) Gascón, J. A.; Sproviero, E. M.; Batista, V. S. Computational Studies of the Primary Phototransduction Event in Visual Rhodopsin. *Acc. Chem. Res.* **2006**, *39*, 184−193. (e) Rivalta, I.; Nenov, A.; Garavelli, M. Modelling retinal chromophores photoisomerization: from minimal models in vacuo to ultimate bidimensional spectroscopy in rhodopsins. *Phys. Chem. Chem. Phys.* **2014**, *16*, 16865−16879.

(16) Reed, A. E.; Curtiss, L. A.; Weinhold, F. Intermolecular Interactions from a Natural Bond Orbital, Donor-Acceptor Viewpoint. *Chem. Rev.* **1988**, *88*, 899−926.

(17) Gascon, J. A.; Batista, V. S. *Biophys. J.* **2004**, *87* (5), 2931−2941.

(18) Palczewski, K.; Kumasaka, T.; Hori, T.; Behnke, C. A.; Motoshima, H.; Fox, B. A.; Trong, I. L.; Teller, D. C.; Okada, T.; Stenkamp, R. E.; Yamamoto, M.; Miyano, M. Crystal Structure of Rhodopsin: A G Protein-Coupled Receptor. *Science* **2000**, *289*, 739−745.

(19) Okada, T.; Fujiyoshi, Y.; Silow, M.; Navarro, J.; Landau, E. M.; Shichida, Y. Functional role of internal water molecules in rhodopsin revealed by x-ray crystallography. *Proc. Natl. Acad. Sci. U.S.A.* **2002**, *99*, 5982−5987.

(20) Fahmy, K.; Jäger, F.; Beck, M.; Zvyaga, T. A.; Sakmar, T. P.; Siebert, F. Protonation states of membrane-embedded carboxylic acid groups in rhodopsin and metarhodopsin II: a Fourier-transform infrared spectroscopy study of site-directed mutants. *Proc. Natl. Acad. Sci. U.S.A.* **1993**, *90*, 10206−10210.

(21) Yan, E. C. Y.; Kazmi, M. A.; De, S.; Chang, B. S. W.; Seibert, C.; Marin, E. P.; Mathies, R. A.; Sakmar, T. P. Function of Extracellular Loop 2 in Rhodopsin: Glutamic Acid 181 Modulates Stability and Absorption Wavelength of Metarhodopsin. *Biochemistry* **2002**, *41*, 3620−3627.

(22) (a) Lüdeke, S.; Beck, M.; Yan, E. C. Y.; Sakmar, T. P.; Siebert, F.; Vogel, R. The Role of Glu181 in the Photoactivation of Rhodopsin. *J. Mol. Biol.* **2005**, *353*, 345−356. (b) Frähmcke, J. S.; Wanko, M.; Phatak, P.; Mroginski, M. A.; Elstner, M. The Protonation State of Glu181 in Rhodopsin Revisited: Interpretation of Experimental Data on the Basis of QM/MM Calculations. *J. Phys. Chem. B* **2010**, *114*, 11338−11352. (c) Valsson, O.; Campomanes, P.; Tavernelli, I.; Rothlisberger, U.; Filippi, C. Rhodopsin Absorption from First

DOI: 10.1021/ct500612n
J. Chem. Theory Comput. 2015, 11, 1206−1219

Principles: Bypassing Common Pitfalls. *J. Chem. Theory Comput.* **2013**, *9*, 2441−2454. (d) Ahuja, S.; Eilers, M.; Hirshfeld, A.; Yan, E. C. Y.; Ziliox, M.; Sakmar, T. P.; Sheves, M.; Smith, S. O. 6-s-cis Conformation and Polar Binding Pocket of the Retinal Chromophore in the Photoactivated State of Rhodopsin. *J. Am. Chem. Soc.* **2009**, *131*, 15160−15169.

(23) (a) Nagata, T.; Terakita, A.; Kandori, H.; Shichida, Y.; Maeda, A. The Hydrogen-Bonding Network of Water Molecules and the Peptide Backbone in the Region Connecting Asp83, Gly120, and Glu113 in Bovine Rhodopsin. *Biochemistry* **1998**, *37*, 17216−17222. (b) Yan, E. C. Y.; Kazmi, M. A.; Ganim, Z.; Hou, J.-M.; Pan, D.; Chang, B. S. W.; Sakmar, T. P.; Mathies, R. A. Retinal counterion switch in the photoactivation of the G protein-coupled receptor rhodopsin. *Proc. Natl. Acad. Sci. U.S.A.* **2003**, *100*, 9262−9267. (c) Sekharan, S.; Mooney, V. L.; Rivalta, I.; Kazmi, M. A.; Neitz, M.; Neitz, J.; Sakmar, T. P.; Yan, E. C. Y.; Batista, V. S. Spectral Tuning of Ultraviolet Cone Pigments: An Interhelical Lock Mechanism. *J. Am. Chem. Soc.* **2013**, *135*, 19064−19067. (d) Strambi, A.; Coto, P.; Ferré, N.; Olivucci, M. Effects of water re-location and cavity trimming on the CASPT2//CASSCF/AMBER excitation energy of Rhodopsin. *Theor. Chem. Acc.* **2007**, *118*, 185−191. (e) Melaccio, F.; Olivucci, M.; Lindh, R.; Ferré, N. Unique QM/MM potential energy surface exploration using microiterations. *Int. J. Quantum Chem.* **2011**, *111*, 3339−3346.

(24) Röhrig, U. F.; Sebastiani, D. NMR Chemical Shifts of the Rhodopsin Chromophore in the Dark State and in Bathorhodopsin: A Hybrid QM/MM Molecular Dynamics Study. *J. Phys. Chem. B* **2008**, *112*, 1267−1274.

(25) Dapprich, S.; Komaromi, I.; Byun, K. S.; Morokuma, K.; Frisch, M. J. *J. Mol. Struct. THEOCHEM* **1999**, *461*, 1−21.

(26) Frisch, M. J.; Trucks, G. W.; Schlegel, H. B.; Scuseria, G. E.; Robb, M. A.; Cheeseman, J. R.; Montgomery, J. A., Jr.; Vreven, T.; Kudin, K. N.; Burant, J. C.; Millam, J. M.; Iyengar, S. S.; Tomasi, J.; Barone, V.; Mennucci, B.; Cossi, M.; Scalmani, G.; Rega, N.; Petersson, G. A.; Nakatsuji, H.; Hada, M.; Ehara, M.; Toyota, K.; Fukuda, R.; Hasegawa, J.; Ishida, M.; Nakajima, T.; Honda, Y.; Kitao, O.; Nakai, H.; Klene, M.; Li, X.; Knox, J. E.; Hratchian, H. P.; Cross, J. B.; Bakken, V.; Adamo, C.; Jaramillo, J.; Gomperts, R.; Stratmann, R. E.; Yazyev, O.; Austin, A. J.; Cammi, R.; Pomelli, C.; Ochterski, J. W.; Ayala, P. Y.; Morokuma, K.; Voth, G. A.; Salvador, P.; Dannenberg, J. J.; Zakrzewski, V. G.; Dapprich, S.; Daniels, A. D.; Strain, M. C.; Farkas, O.; Malick, D. K.; Rabuck, A. D.; Raghavachari, K.; Foresman, J. B.; Ortiz, J. V.; Cui, Q.; Baboul, A. G.; Clifford, S.; Cioslowski, J.; Stefanov, B. B.; Liu, G.; Liashenko, A.; Piskorz, P.; Komaromi, I.; Martin, R. L.; Fox, D. J.; Keith, T.; Al-Laham, M. A.; Peng, C. Y.; Nanayakkara, A.; Challacombe, M.; Gill, P. M. W.; Johnson, B.; Chen, W.; Wong, M. W.; Gonzalez, C.; Pople, J. A. *Gaussian 03*, revision A3; Gaussian, Inc.: Wallingford, CT, 2004.

(27) Groesbeek, M.; Rood, G. A.; Lugtenburg, J. *Recl. Trav. Chim. Pays-Bas* **1992**, *111*, 149−154.

(28) Elia, G. R.; Childs, R. F.; Britten, J. F.; Yang, D. S. C.; Santarsiero, B. D. *Can. J. Chem.* **1996**, *74*, 591.

(29) Miertus, S.; Scrocco, E.; Tomasi, J. *Chem. Phys.* **1981**, *55*, 117.

(30) (a) Ramsey, N. F. Magnetic Shielding of Nuclei in Molecules. *Phys. Rev.* **1950**, *78*, 699−703. (b) Ramsey, N. F. Electron Coupled Interactions between Nuclear Spins in Molecules. *Phys. Rev.* **1953**, *91*, 303−307.

(31) London, F. The quantic theory of inter-atomic currents in aromatic combinations. *J. Phys. Radium* **1937**, *8*, 397−409.

(32) Wolinski, K.; Hilton, J. F.; Pulay, P. *J. Am. Chem. Soc.* **1990**, *112*, 8251.

(33) Ditchfield, R. On molecular orbital theories of NMR chemical shifts. *Chem. Phys. Lett.* **1972**, *15*, 203−206.

(34) Ramsey, N. F. *Phys. Rev.* **1953**, *91*, 303.

(35) Contreras, R. H.; Peralta, J. E.; Giribet, C. G.; Ruiz de azúa, M. C.; Facelli, J. C., Advances in theoretical and physical aspects of spin-spin coupling constants. In *Annual Reports on NMR Spectroscopy*; Academic Press: 2000; Vol. *41*, pp 55−184.

(36) Sychrovsky, V.; Gräfenstein, J.; Cremer, D. J. *J. Chem. Phys.* **2000**, *113*, 3530−3547.

(37) Helgaker, T.; Watson, M.; Handy, N. C. *J. Chem. Phys.* **2000**, *113*, 9402.

(38) Contreras, R. H.; Barone, V.; Facelli, J. C.; Peralta, J. E. *Annu. Rep. NMR Spectrosc.* **2003**, *51*, 167.

(39) Becke, A. D. *J. Chem. Phys.* **1993**, *98*, 5648.

(40) Lai, W. C.; McLean, N.; Gansmüller, A.; Verhoeven, M. A.; Antonioli, G. C.; Carravetta, M.; Duma, L.; Bovee-Geurts, P. H. M.; Johannessen, O. G.; de Groot, H. J. M.; Lugtenburg, J.; Emsley, L.; Brown, S. P.; Brown, R. C. D.; DeGrip, W. J.; Levitt, M. H. Measurement of 13C-13C J-couplings in the Rhodopsin Chromophore by Double-Quantum Solid-State NMR Spectroscopy. *J. Am. Chem. Soc.* **2006**, *128*, 3878−3879.

(41) Peralta, J. E.; Scuseria, G. E.; Cheeseman, J. R.; Frisch, M. *J. Phys. Chem. Lett.* **2003**, *375*, 452.

(42) Thom, H.; Dunning, J. *J. Chem. Phys.* **1988**, *90*, 1007−1023.

(43) Woon, D. E.; Thom, H.; Dunning, J. *J. Chem. Phys.* **1995**, *103*, 4572−4585.

(44) (a) Glendening, E. D.; Weinhold, F. Natural resonance theory: I. General formalism. *J. Comput. Chem.* **1998**, *19*, 593−609. (b) Glendening, E. D.; Weinhold, F. Natural Resonance Theory: II. Natural bond order and valency. *J. Comput. Chem.* **1998**, *19*, 610−627. (c) Glendening, E. D.; Badenhoop, J. K.; Weinhold, F. Natural resonance theory: III. Chemical applications. *J. Comput. Chem.* **1998**, *19*, 628−646.

(45) Sproviero, E. M.; Pophristic, V. Intramolecular Natural Energy Decomposition Analysis. Applications to rational design of foldamers. *J. Chem. Phys.* **2014**, Submitted.

(46) (a) Glendening, E. D.; Streitwieser, A. Natural energy decomposition analysis: An energy partitioning procedure for molecular interactions with application to weak hydrogen bonding, strong ionic, and moderate donor–acceptor interactions. *J. Chem. Phys.* **1994**, *100*, 2900−2909. (b) Schenter, G. K.; Glendening, E. D. Natural Energy Decomposition Analysis: The Linear Response Electrical Self Energy. *J. Phys. Chem.* **1996**, *100*, 17152−17156. (c) Glendening, E. D. Natural Energy Decomposition Analysis: Explicit Evaluation of Electrostatic and Polarization Effects with Application to Aqueous Clusters of Alkali Metal Cations and Neutrals. *J. Am. Chem. Soc.* **1996**, *118*, 2473−2482.

(47) (a) Schmidt, M. W.; Baldridge, K. K.; Boatz, J. A.; Elbert, S. T.; Gordon, M. S.; Jensen, J. H.; Koseki, S.; Matsunaga, N.; Nguyen, K. A.; Su, S.; Windus, T. L.; Dupuis, M.; Montgomery, J. A. General atomic and molecular electronic structure system. *J. Comput. Chem.* **1993**, *14*, 1347−1363. (b) Gordon, M. S.; Schmidt, M. W., Advances in electronic structure theory: GAMESS a decade later. In *Advances in Electronic Structure Theory: GAMESS a Decade Late*, Dykstra, C. E.; Frenking, G.; Kim, K. S.; Scuseria, G. E., Eds.; Elsevier: Amsterdam, 2005; pp 1167−1189.

(48) (a) Feng, X.; Verdegem, P. J. E.; Lee, Y. K.; Sandström, D.; Edén, M.; Bovee-Geurts, P.; de Grip, W. J.; Lugtenburg, J.; de Groot, H. J. M.; Levitt, M. H. Direct Determination of a Molecular Torsional Angle in the Membrane Protein Rhodopsin by Solid-State NMR. *J. Am. Chem. Soc.* **1997**, *119*, 6853−6857. (b) Verdegem, P. J. E.; Bovee-Geurts, P. H. M.; de Grip, W. J.; Lugtenburg, J.; de Groot, H. J. M. Retinylidene Ligand Structure in Bovine Rhodopsin, Metarhodopsin-I, and 10-Methylrhodopsin from Internuclear Distance Measurements Using 13C-Labeling and 1-D Rotational Resonance MAS NMR. *Biochemistry* **1999**, *38*, 11316−11324. (c) Wang, Q.; Kochendoerfer, G. G.; Schoenlein, R. W.; Verdegem, P. J. E.; Lugtenburg, J.; Mathies, R. A.; Shank, C. V. Femtosecond Spectroscopy of a 13-Demethylrhodopsin Visual Pigment Analogue: The Role of Non-bonded Interactions in the Isomerization Process. *J. Phys. Chem.* **1996**, *100*, 17388−17394. (d) Palings, I.; Pardoen, J. A.; Van den Berg, E.; Winkel, C.; Lugtenburg, J.; Mathies, R. A. Assignment of fingerprint vibrations in the resonance Raman spectra of rhodopsin, isorhodopsin, and bathorhodopsin: implications for chromophore structure and environment. *Biochemistry* **1987**, *26*, 2544−2556.

DOI: 10.1021/ct500612n
J. Chem. Theory Comput. 2015, 11, 1206−1219

(49) (a) Blizzard, A. C.; Santry, D. P. *J. Chem. Phys.* **1971**, *55*, 1950. (b) Contreras, R. H.; Peralta, J. E. *Prog. Nucl. Magn. Reson. Spectrosc.* **2000**, *37*, 321.
(50) Touw, S. I. E.; de Groot, H. J. M.; Buda, F. Ab Initio Modeling of the Spatial, Electronic, and Vibrational Structure of Schiff Base Models for Visual Photoreceptors. *J. Phys. Chem. B* **2004**, *108*, 13560−13572.
(51) Buda, F.; Giannozzi, P.; Mauri, F. Density Functional Theory Study of the Structure and 13C Chemical Shifts of Retinylidene Iminium Salts. *J. Phys. Chem. B* **2000**, *104*, 9048−9053.
(52) (a) Engelmann, A. R.; Scuseria, G. E.; Contreras, R. H. The Use of Partially Restricted Molecular-Orbitals to Investigate Transmission Mechanisms of Spin Spin Coupling-Constants. 2. The Sigma-Contribution and Pi-Contribution to the Fermi Contact, Orbital, and Spin Dipolar Terms of Scpt Indo C-C Coupling-Constants. *J. Magn. Reson.* **1982**, *50*, 21−29. (b) Grafenstein, J.; Tuttle, T.; Cremer, D. Decomposition of nuclear magnetic resonance spin-spin coupling constants into active and passive orbital contributions. *J. Chem. Phys.* **2004**, *120*, 9952−9968.
(53) Grafenstein, J.; Tuttle, T.; Cremer, D. Analysis of long-range NMR spin-spin coupling in polyenes and the pi-mechanism. *Phys. Chem. Chem. Phys.* **2005**, *7*, 452−462.
(54) (a) Bifone, A.; de Groot, H. J. M.; Buda, F. Energy Storage in the Primary Photoproduct of Vision. *J. Phys. Chem. B* **1997**, *101*, 2954−2958. (b) González-Luque, R.; Garavelli, M.; Bernardi, F.; Merchán, M.; Robb, M. A.; Olivucci, M. Computational evidence in favor of a two-state, two-mode model of the retinal chromophore photoisomerization. *Proc. Natl. Acad. Sci. U.S.A.* **2000**, *97*, 9379−9384.
(55) Carey, F.; Giuliano, R. *Organic Chemistry*, 9th ed.; McGraw-Hill Higher Education: New York, 2013.
(56) Verhoeven, M. A.; Creemers, A. F. L.; Bovee-Geurts, P. H. M.; De Grip, W. J.; Lugtenburg, J.; de Groot, H. J. M. Ultra-High-Field MAS NMR Assay of a Multispin Labeled Ligand Bound to Its G-Protein Receptor Target in the Natural Membrane Environment: Electronic Structure of the Retinylidene Chromophore in Rhodopsin. *Biochemistry* **2001**, *40*, 3282−3288.
(57) (a) Garavelli, M.; Celani, P.; Bernardi, F.; Robb, M. A.; Olivucci, M. The C5H6NH2+ Protonated Shiff Base: An ab Initio Minimal Model for Retinal Photoisomerization. *J. Am. Chem. Soc.* **1997**, *119*, 6891−6901. (b) Vreven, T.; Bernardi, F.; Garavelli, M.; Olivucci, M.; Robb, M. A.; Schlegel, H. B. Ab Initio Photoisomerization Dynamics of a Simple Retinal Chromophore Model. *J. Am. Chem. Soc.* **1997**, *119*, 12687−12688.

DOI: 10.1021/ct500612n
J. Chem. Theory Comput. 2015, 11, 1206−1219